Quarterly Progress Report No. 2

INVESTIGATION OF ELECTRON EMISSION CHARACTERISTICS OF LOW WORK FUNCTION SURFACES

by

L. W. Swanson
L. C. Crouser

Prepared for

Headquarters
National Aeronautics and Space Administration
Washington, D. C.

CONTRACT NASw-1082

Field Emission Corporation
McMinnville, Oregon

Quarterly Progress Report No. 2
for the Period
28 December 1964 to 31 March 1965

INVESTIGATION OF ELECTRON EMISSION CHARACTERISTICS OF LOW WORK FUNCTION SURFACES

by

L. W. Swanson
L. C. Crouser

Prepared for

Headquarters
National Aeronautics and Space Administration
Washington, D. C.

6 May 1965

CONTRACT NASw-1082

FIELD EMISSION CORPORATION
Melrose Avenue at Linke Street
McMinnville, Oregon 97128

TABLE OF CONTENTS

LIST OF ILLUSTRATIONS

PURPOSE

The primary aims of this investigation are to obtain an improved fundamental understanding of (1) the phenomena governing the production of low work function surfaces, and (2) the factors affecting the quality and stability of electron emission characteristics. It is expected that the information generated from this investigation will be relevant to various kinds of electron emission (i.e., photo, thermionic and field emission), although the primary emphasis will be placed upon field emission. Accordingly, field emission techniques will be employed, at least initially, to obtain the objectives of this work.

The formation of low work function surfaces will be accomplished by; (1) adsorption of appropriate electro-positive adsorbates, (2) co-adsorption of appropriate electro-positive and electro-negative adsorbates, and (3) fabrication of emitters of low work function surfaces from various metalloid compounds. Various properties of these surfaces to be investigated in order to obtain a more fundamental understanding of them are the temperature dependency of the emission and work function, the various types of energy exchanges accompanying emission, the energy distribution of the field emitted electron, and various aspects of the surface kinetics of adsorbed layers such as binding energy, surface mobility and effect of external fields.

29144

ABSTRACT

A preliminary investigation of the total energy distribution of field emitted electrons has been performed in the temperature range 77 - 1059°K. The results obtained confirm the theoretically predicted inversion temperature and support the general features of the free-electron model for tungsten.

Measurements of the energy exchange accompanying field emission on clean tungsten have been repeated under more ideal conditions and show striking deviations from theory. Although the general qualitative features of the existing theory of "Nottingham" emission heating and cooling were confirmed, certain discrepancies were noted between experiment and theory in regard to the amount of energy exchange per electron and the value of the temperature boundary which separates emission heating and cooling. The discrepancies between the inversion temperatures determined by measurements of the total energy distribution and the Nottingham effect may be due to a preponderance of conduction by holes below the Fermi level. It is further suggested that confirmation of the free-electron model of tungsten by the energy distribution results may be somewhat fortuitous and that a two-band electronic structure containing holes and electrons may be more proper for tungsten.

An analysis of the work function vs. cesium coverage results on the (100) and the (110) planes of tungsten has been made and suggests a surface polarizability for cesium between 5 and 7 A^3 for the two planes. Author

ture. Further investigations of the energy distribution from various crystallographic directions and in the presence of adsorbates such as zirconium are being performed.

TOTAL ENERGY DISTRIBUTION MEASUREMENTS

The average energy of the emitted electrons and the inversion temperature obtained from investigations of the Nottingham effect can be checked experimentally by comparison with corresponding experimentally determined total energy distributions. A preliminary investigation has been made of the total energy distribution of field emitted electrons from clean tungsten over the temperature range 77 - 1059°K. Because of the importance of these results in shedding light on discrepancies between experimental and calculated values of the Nottingham effect, a brief description of the tube and preliminary results of the total energy distribution measurements will be given.

EXPERIMENTAL TECHNIQUES AND PROCEDURES

The energy analyzer tube utilized in this investigation was based on a design by Dr. van Oostrom of the Phillips Laboratory and is shown in Figure 1. Briefly, the tube is designed in such a way that electrons passing through the lens system are focused near the center of the spherical collector F. The electrode system of the analyzer consists of an anode D, a lens electrode E and a Faraday cage G. The latter electrode is operated near ground potential and acts as a shielding electrode for the hemispherical collector (also operating near ground potential) and accordingly reduces the

PROGRESS TO DATE

Progress is being made in four general areas of investigation of low work function surfaces obtained by electro-positive metallic adsorption on tungsten and co-adsorption. They are: (1) emission heating; (2) energy distribution; (3) surface kinetics; (4) work function change on single crystallographic planes. The investigation of the preceding phenomena each involves different tube embodiments which have been constructed and are currently being used to obtain results. Prior to the commencement of this investigation preliminary results were obtained on various aspects of work function change due to cesium adsorption and co-adsorption with oxygen on tungsten. Some of these results, which have been reported elsewhere[1], will be analyzed in this report.

During this quarter measurements of the energy exchange phenomena accompanying field emission on clean tungsten have been repeated under better conditions. The results so obtained show considerable deviation from theory, particularly at low electric fields and elevated temperatures. At low temperatures and high fields the experimental and calculated results agree more closely. An attempt to measure the energy exchange phenomena over a range of work functions by depositing barium on the emitter was not successful and will be repeated with a thoriated tungsten emitter in order to dispense with a separate source for the adsorbate.

A preliminary investigation of the total energy distribution of field emitted electrons has been completed in the temperature range 77 - 1059°K. The results generally confirm the theoretically predicted inversion tempera-

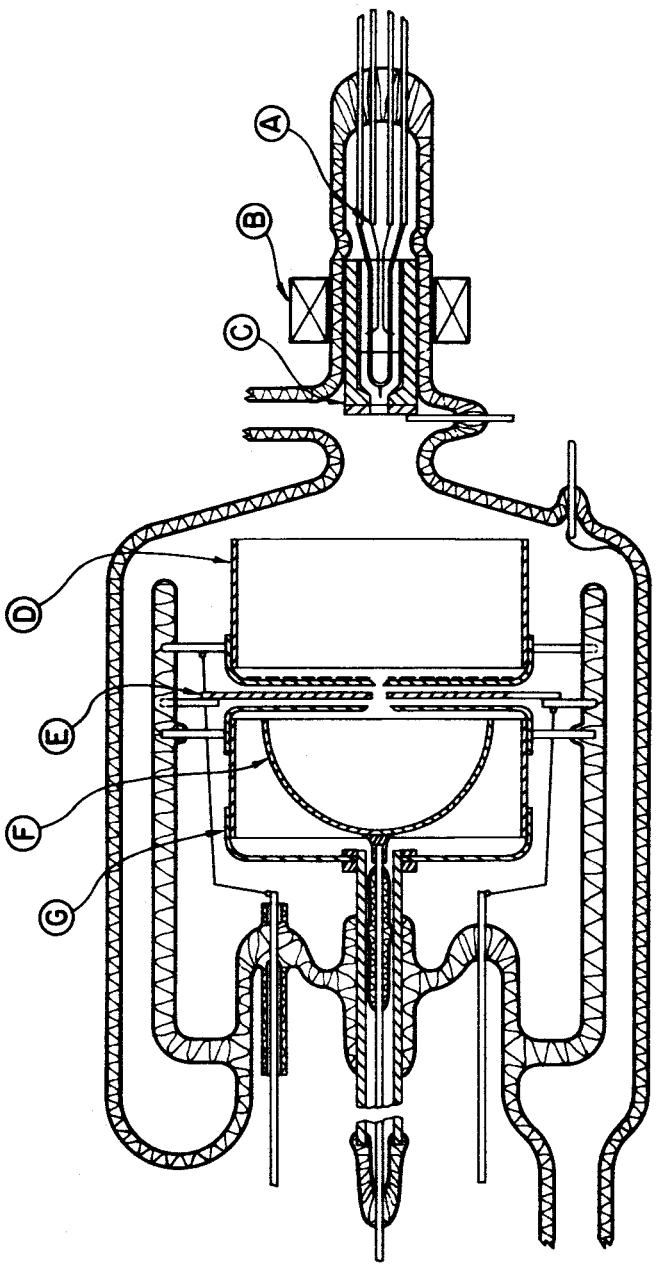

Figure 1. Diagram of energy analyzer tube utilized for measuring total energy distributions from tungsten at various temperatures.

effect of undesirable reflection inherent in most retarding potential analyzers. It should be noted that an electron passing through the cross-over formed near the center of the hemispherical collector will have normal incidence at the collector surface so that the total energy of the emitted electrons will be analyzed.

In practice, the anode potential V_A is constant and the focal length adjusted by varying the potential of the lens electrode V_L. The total energy distribution curves are taken for fixed values of V_L and V_A by varying the cathode potential between -4.0 and -5.5 v, depending upon the work function of the collector. The ratio of V_L to V_A is a critical quantity and for this particular lens system best results were obtained with $V_L/V_A = 0.001$.

The emitter assembly A consisted of a field emission tip spot-welded to a 10-mil tungsten filament with 3-mil potential leads utilized to sample the resistance change across a small length of filament in order to accurately measure the emitter temperature. A small external magnet B and internal concentrator C were used to deflect the beam in order to position the emission from the desired crystallographic plane on the aperture of the anode D. With this arrangement, the tube can not only measure energy distributions from different crystallographic planes but work function variations from plane to plane as well. The I-V data for work function measurements were obtained with the tip at -8 volts and a constant ratio of V_L/V_A in order that the electron trajectories through the lens would be constant over the voltage range. During the I-V measurements with magnetic deflection, compensation of the magnet current must be performed in

order to maintain a constant position of the desired crystallographic plane on the aperture over the voltage range.

The aperturing of the primary beam was sufficient to cause a ratio of the collected current to the total emitted current of $\sim 10^{-3}$ when probing the emission from a low work function region of the emitter. The value of the collected current ranged from 10^{-9} to 10^{-14} amps and was measured by a Cary vibrating reed electrometer with an x-y recorder read-out. The energy distribution curves were obtained by graphical differentiation of the collected current vs. tip voltage curves or, in some cases, the differentiation was performed electronically. A block circuit diagram of the energy distribution tube is given in Figure 2. Total energy distributions are obtained by measuring the collected current I_p as a function of the tip voltage relative to ground. The energy sorting is done by the work function barrier of the collector, so that it is necessary to raise the tip to approximately -4.5 volts (the work function of the collector) before a measurable collected current can be detected. The width of the energy distribution curves are such that the total curve can be measured within one volt. In practice, the collected current I_p is plotted against emitter bias voltage V_t on an x-y recorder. In order to electronically differentiate the integral curves, a 1000 cps signal is applied to the emitter circuit and detected in the collected current I_p with a narrow band 1000 cps amplifier. The magnitude of the 1000 cps signal at the collector is proportional to the derivative of the I_p vs. V_t curve and is also plotted on an x-y recorder as a function of emitter voltage. The temperature of the emitter is controlled by resistive heating

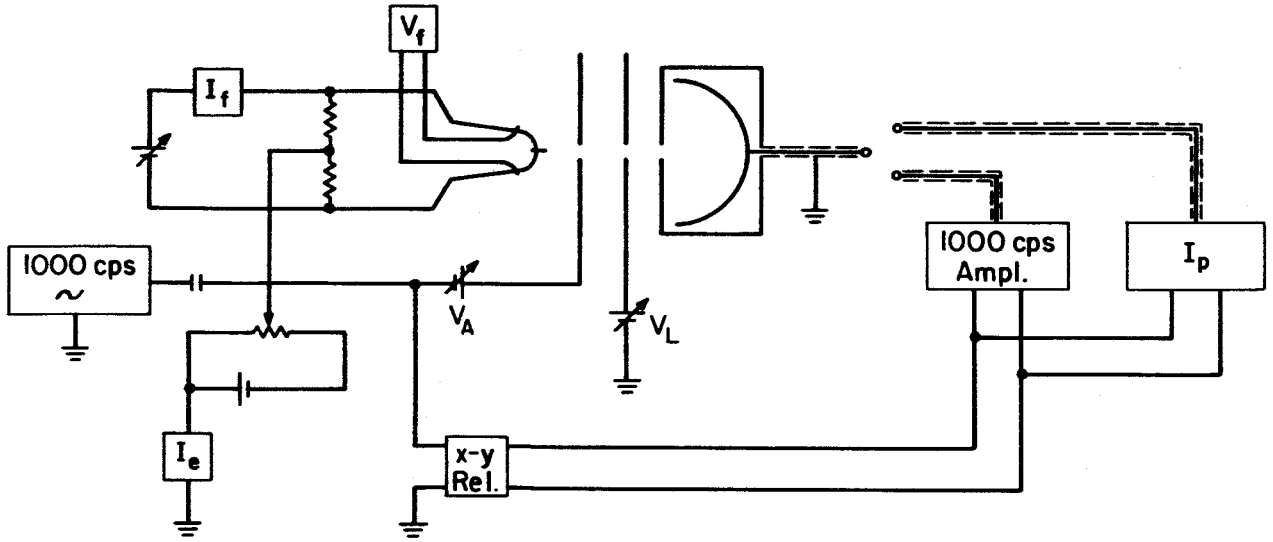

Figure 2. Circuit diagram for energy analyzer tube.

of the emitter support filament with an isolated dc supply as shown in the diagram of Figure 2. Care is taken to insure that IR drops across the filament will not alter the tip bias voltage.

THEORY

In order to more clearly understand the exchange phenomena accompanying field emission, it is instructive to first consider the energy distribution $P(\epsilon)d\epsilon$ and the average energy $\bar{\epsilon} = \bar{E} - E_f$ for field emitted electrons. As shown in an earlier report[2], one can formulate the following expression for the number of field emitted electrons whose energy (relative to the Fermi level) lies between ϵ and $\epsilon + d\epsilon$:

$$P(\epsilon)d\epsilon = \frac{4\pi m d e^{-c} e^{\epsilon/d}}{h^3 (e^{\epsilon/kT} + 1)} d\epsilon \qquad (1)$$

where:

$$c = \frac{4}{3} \frac{(2m\phi^3)^{1/2}}{\hbar e F} v(y) \qquad (2)$$

$$d = \frac{\hbar e F}{2(2m\phi)^{1/2} t(y)} \qquad (3)$$

and $t(y)$ and $v(y)$ are slowly varying functions of ϕ and F which have been published in tabular form[3]. The derivation leading to equation (1) was based on the Sommerfeld-Hartree model of the electronic structure for the metal and shows that the total energy distribution function is a product of the Fermi-Dirac distribution function by a transmission coefficient dependent on field and work function. Multiplying equation (1) by the electronic

equation (6) predicts a dependency of $\bar{\epsilon}$ on T, F and ϕ; it is also apparent that $\bar{\epsilon} = 0$ when $p = 1/2$. Physically, this means that when $p = 1/2$, electrons are emitted from energy levels both above and below the Fermi level with equal probability; or alternatively, the energy distribution predicted by equation (1) is symmetrical about the Fermi level. In fact, it can be shown that the shape of the energy distribution curve of equation (1) depends only on the numerical value of the dimensionless parameter p.

The significance of the condition $p = 1/2$ is that there will be no net energy exchange during emission if the holes left in the conduction band by the emitted electrons are filled by electrons possessing energy at or very near the Fermi level. Whether holes are in fact filled by electrons with the Fermi energy, and furthermore whether this process occurs near the emitting surface, has been the subject of controversy in the past. Both experimental results and theoretical considerations of the mean free path for electron-electron and electron-phonon interactions for electrons (or holes) near the Fermi energy suggest the occurrence of such energy exchange processes within the dimensions of an emitter tip, which is the order of 10^{-5} cm.

From the preceding considerations one can define an inversion temperature T^* for which the energy distribution is symmetrical about the Fermi level:

$$T^* = \frac{d}{2k} = \frac{5.67 \times 10^{-5} F}{t(y) \phi^{1/2}} \quad (^{\circ}K) \qquad (7)$$

for F in V/cm and ϕ in ev. Thus, the inversion temperature is a function of

charge, then integrating over the limits $-\infty$ to ∞ yields an expression for the current density of the field emitted electrons. This integration is conveniently accomplished by defining a dimensionless parameter $p = kT/d$ which leads to an expression for the current density J_{TF} of T-F emission of the following form:

$$J_{TF} = \frac{\pi p}{\sin \pi p} \frac{F^2 e^{-c}}{8\pi h \phi t^2 (y)} = \frac{\pi p}{\sin \pi p} J_{0F} \qquad (4)$$

which breaks down completely at $p = 1$ but is approximately valid up to $p = 2/3$. For small values of p (i.e., low temperatures or high field) $\pi p / \sin \pi p \cong 1$ and one obtains the $0^{\circ}K$ approximation of the Fowler-Nordheim formula J_{0F}.

With an analytical expression for the total energy distribution it is possible to obtain an expression for the average energy $\bar{\epsilon}$ of the field emitted electrons by performing the following integration:

$$\bar{\epsilon} = \frac{\int_{-\infty}^{\infty} \epsilon P(\epsilon)\, d\epsilon}{\int_{-\infty}^{\infty} P(\epsilon)\, d\epsilon} = -d f(p) \qquad (5)$$

where f(p) is unity at $p = 0$, zero at $p = 1/2$ and negative for $p > 1/2$. Levine[4] has shown that the function $f(p) = \pi p / \tan \pi p$ so that equation (5) may be written in an alternative form:

$$\bar{\epsilon} = -\pi kT \cot \pi p \qquad (6)$$

which is also valid over the approximate range $0 \leq p \leq 2/3$. The form of

F and ϕ and it can be examined experimentally and compared with energy distributions at T^* for experimental self-consistency.

RESULTS AND DISCUSSION

The preliminary energy distribution results obtained thus far are given in Figure 3 and represent emission from a (116) plane with a measured work function of 4.35 ev. The work function of the collector, which also represents the position of the Fermi level, is approximately 4.92 volts and the current per unit energy is arbitrarily normalized such that the maximum for the 384°K results matches the theoretical value given in Figure 4. A comparison of the experimental and theoretical curves based on this normalization procedure shows fairly good agreement, except for the 77°K results where the discrepancy is attributed to the inability of the analyzer to resolve the narrow peak of the 77°K curve. It was later discovered that the reason for the poor resolution of the analyzer was due to a slight error in positioning one of the electrodes. Another fundamental difficulty in obtaining energy distribution results at temperatures above 550°K is the occurrence of appreciable flicker noise in the collected current which complicates the determination of the differentiated curves.

Because of the preliminary nature of the experimental results, a detailed comparison with theory is premature; however, it seems clear that the general behavior of the experimental results is in good accord with theory and that the inversion temperature, which is calculated to occur at 1040°K for the applicable F and ϕ values, is well confirmed by the nearly symmetrical energy distribution curve obtained at 1059°K.

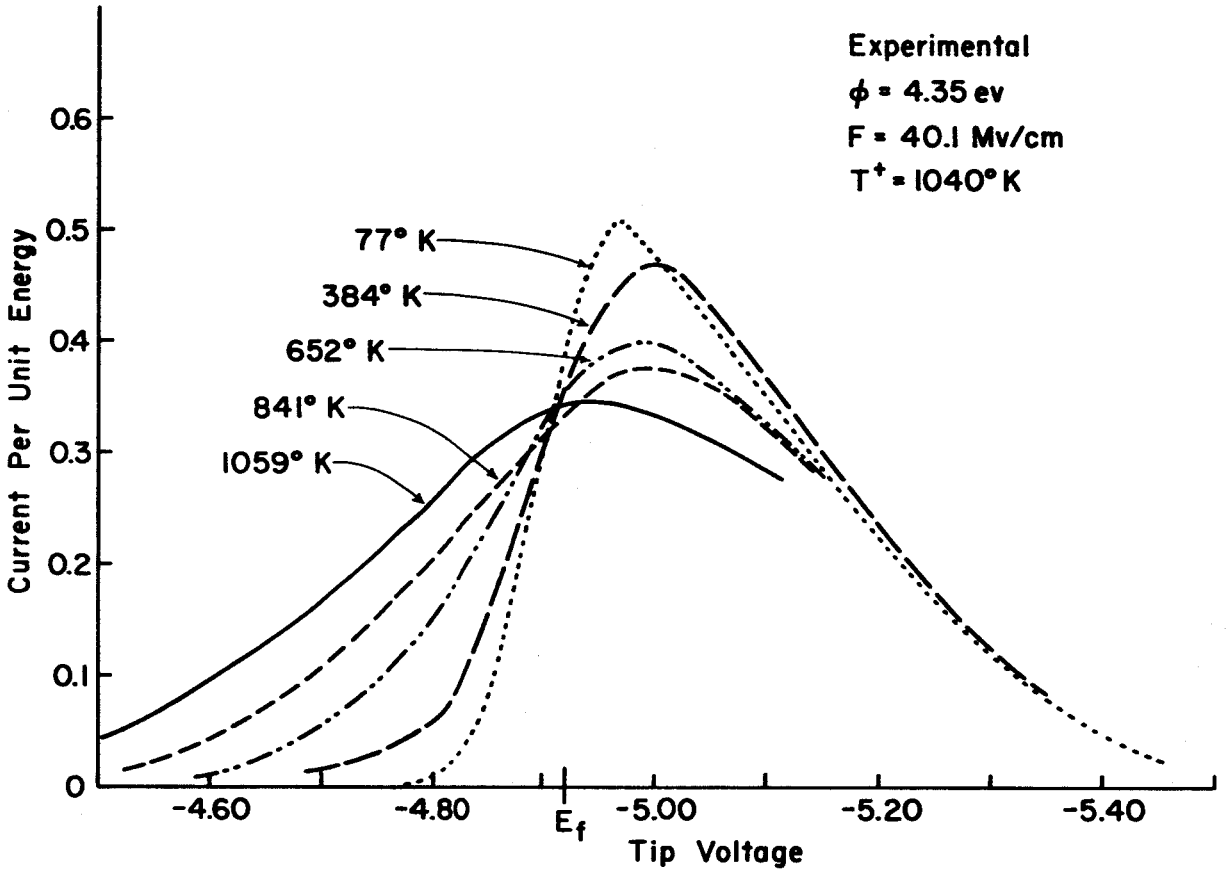

Figure 3. Curves show experimentally determined total energy distribution results at the indicated temperatures. Field emission current measured primarily from (116) plane.

EMISSION HEATING AND COOLING

The energy exchanges accompanying field emission which lead to either heating or cooling of the lattice have been investigated[2] for clean tungsten and zirconium-coated tungsten surfaces. Inversion temperatures and the energy exchange per electron during emission were determined and compared with existing theory. It was noted that the experimental measurements of both the inversion temperatures and the energy exchange per electron deviated considerably from the theoretically predicted values over a wide range of fields and substrate temperatures. Because of the difficult nature of the experiment and the possibilities of certain artifacts of the tube to obscure the absolute values of the measured energy exchange accompanying field emission, the results for clean tungsten were repeated under more ideal conditions and are reported below.

EXPERIMENTAL TECHNIQUES AND PROCEDURES

A description of the tube and its operation have been given in an earlier report[2] and the procedures used to obtain the data reported herein are similar to those described earlier. The zirconium source was replaced by a barium source in this investigation in order to study the emission heating and cooling over a variable range of work functions extending as low as 2.0 ev. In addition, a sharper emitter was employed in order to obtain the desired emission currents at lower total voltage. This is desirable from the standpoint of reducing the power dissipation on the collector plates and thereby reducing the ambient temperature variations in the tube during the measurements. Also, the collector plates were more rigorously outgassed

in order to eliminate the possibility of electron impact ionization of adsorbed layers which leads to ion impact on the emitter structure and erroneous increase of the measured energy input at the emitter structure. The measured power exchange H at the emitter as a function of emitter current I_e is given in Figure 5 for clean tungsten at various temperatures.

RESULTS AND DISCUSSION

Two main observations can be made from the data given in Figure 5: First, it is noted that H increases with I_e in a near-linear fashion at low temperatures; second, it appears that the amount of heating at a given I_e decreases with increasing temperature. Defining a symbol A as the energy per emitted electron exchanged with the lattice (positive A means energy given to the lattice), we can write the following expression:

$$H = I_e A = -\bar{\epsilon} I_e \tag{8}$$

If we further recall that the definition of the inversion temperature can be given as $p = T/2T^*$, then combining equations (6) and (8) one obtains the following expression:

$$H = I_e \pi k T \cot \frac{\pi T}{2T^*} \tag{9}$$

Hence, the two observed experimental trends, namely a near-linear increase of H with I_e and a decrease with T, are predicted by theory. It is further noticed that as T approaches T^* the variation of H with I_e will no longer be near-linear and depends more strongly on the variation of T^* with F and, hence, I_e. When the condition $T = T^*$ is reached, $H = 0$; this is

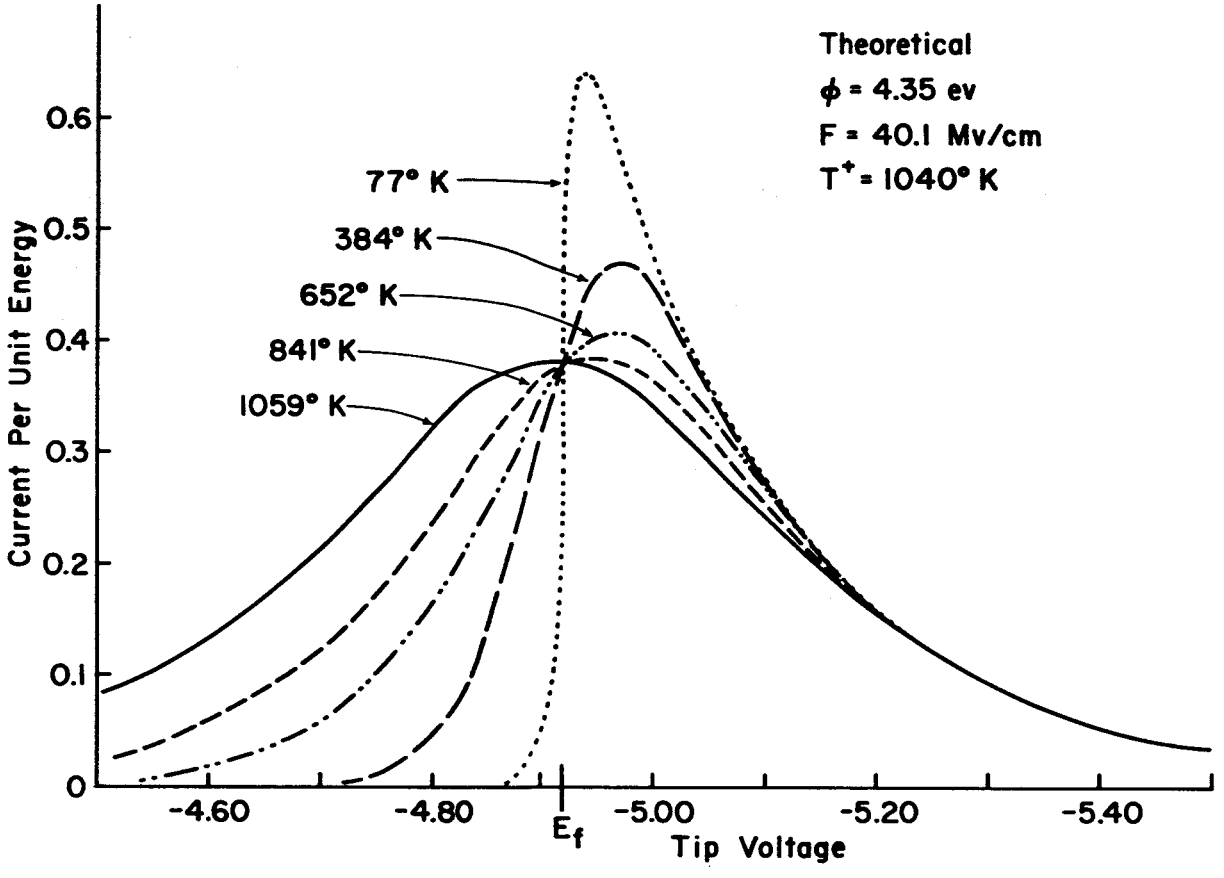

Figure 4. Curves show total energy distribution calculated according to equation (1) which correspond to the experimental results given in Figure 3.

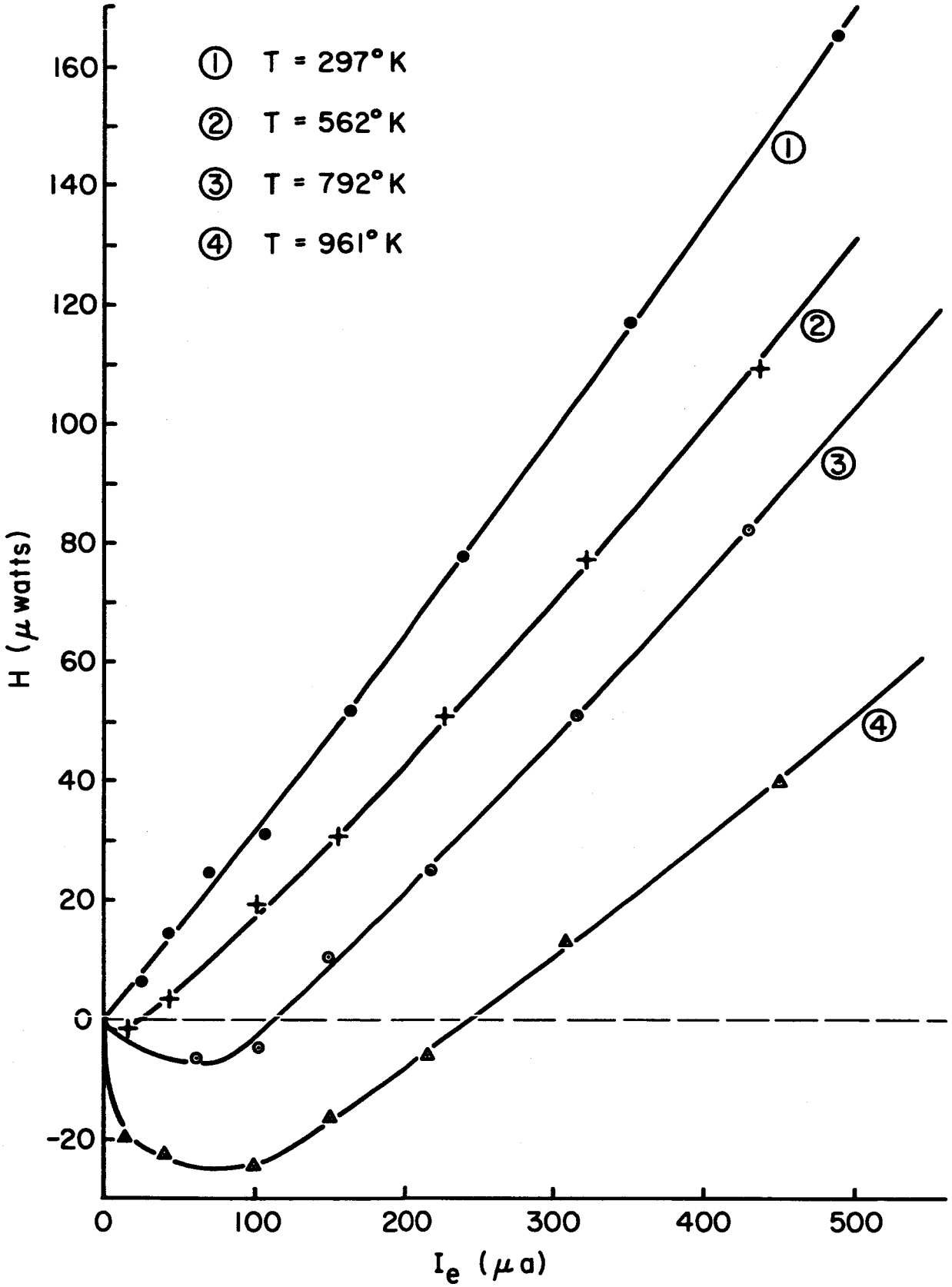

Figure 5. Experimentally determined power exchange H at the emitter as a function of field emitted current I_e at the indicated temperatures for clean tungsten where ϕ = 4.52 ev. Negative values of H indicate emission cooling.

confirmed experimentally in the higher temperature results of Figure 5 which show a transition from emission heating to cooling.

It was possible to measure the value of T^* as a function of F over a limited range of field for both clean and zirconium-coated tungsten. These results, given in Figure 6 along with the expected theoretical variation, clearly show a discrepancy between experimental and calculated values of T^*, although the variation of T^* with F appears to be linear as predicted by theory.

In order to make a quantitative comparison of the experimental results with theory, smooth curves were drawn through the H vs. I_e data, and values of $A = H/I_e$ were plotted against F, as shown in Figure 7. Corresponding calculated curves are given in Figure 8. A comparison of the curves of Figures 7 and 8 show that, whereas the overall qualitative variations of the energy exchange per emitted electron with field and temperature are in the direction predicted by theory, there are some marked quantitative discrepancies between the experimental and theoretically expected results. At 297°K the variation A with F agreed with theory but the experimental values are approximately 50% greater than those predicted by theory. These results agree with those reported earlier. In contrast, the higher temperature results all show much lower values of A than expected by theory at low fields, but at higher fields experimental values of A approach the theoretical values. A further consequence of the experimental results of Figure 7 is the prediction of an inversion temperature considerably below the theoretical value. The latter result was shown more directly in Figure 6, which shows

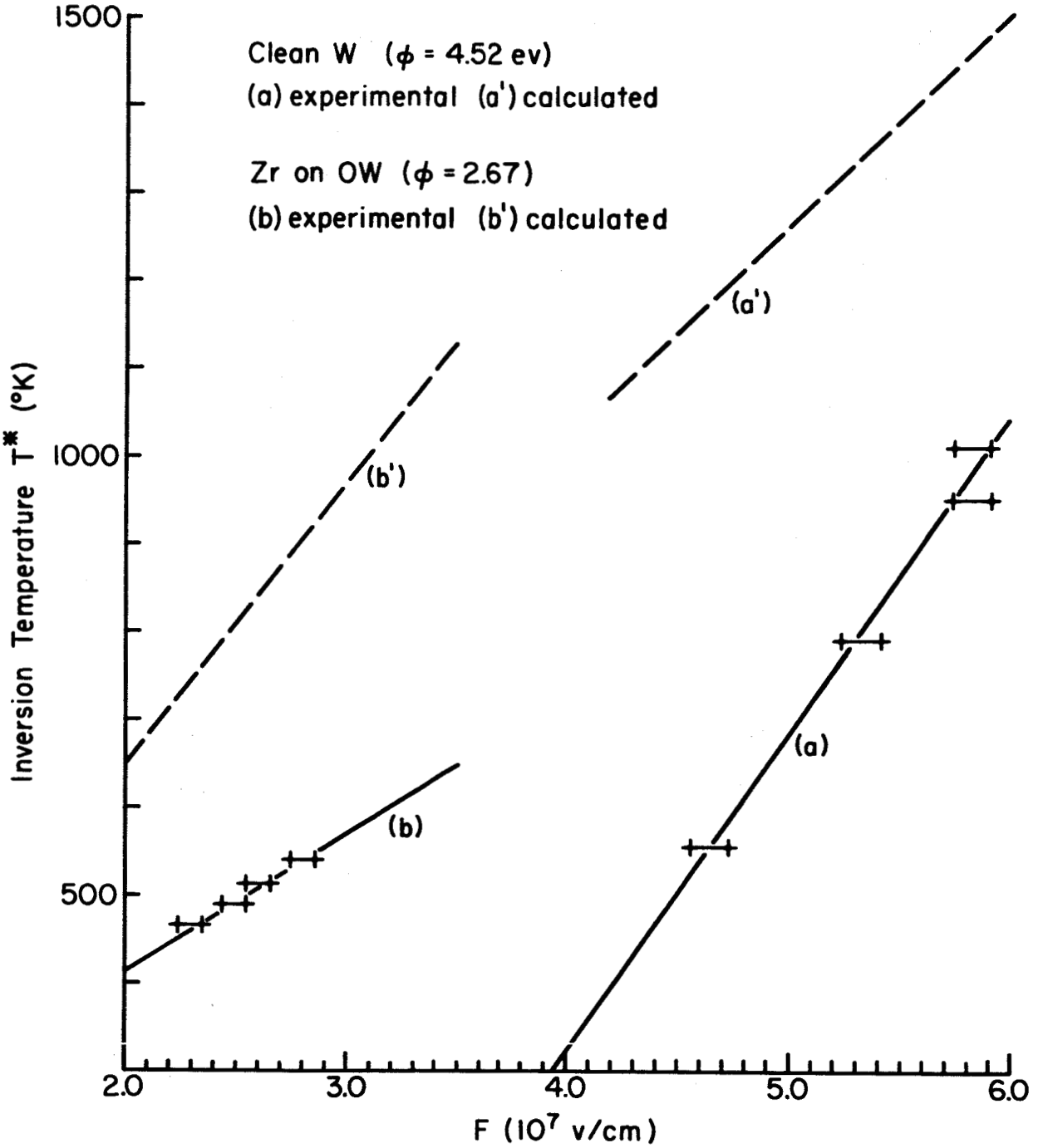

Figure 6. Experimentally determined inversion temperatures T^* for a clean and zirconium-coated tungsten emitter as a function of applied electric field. Dashed curves are the respective calculated inversion temperatures according to equation (7).

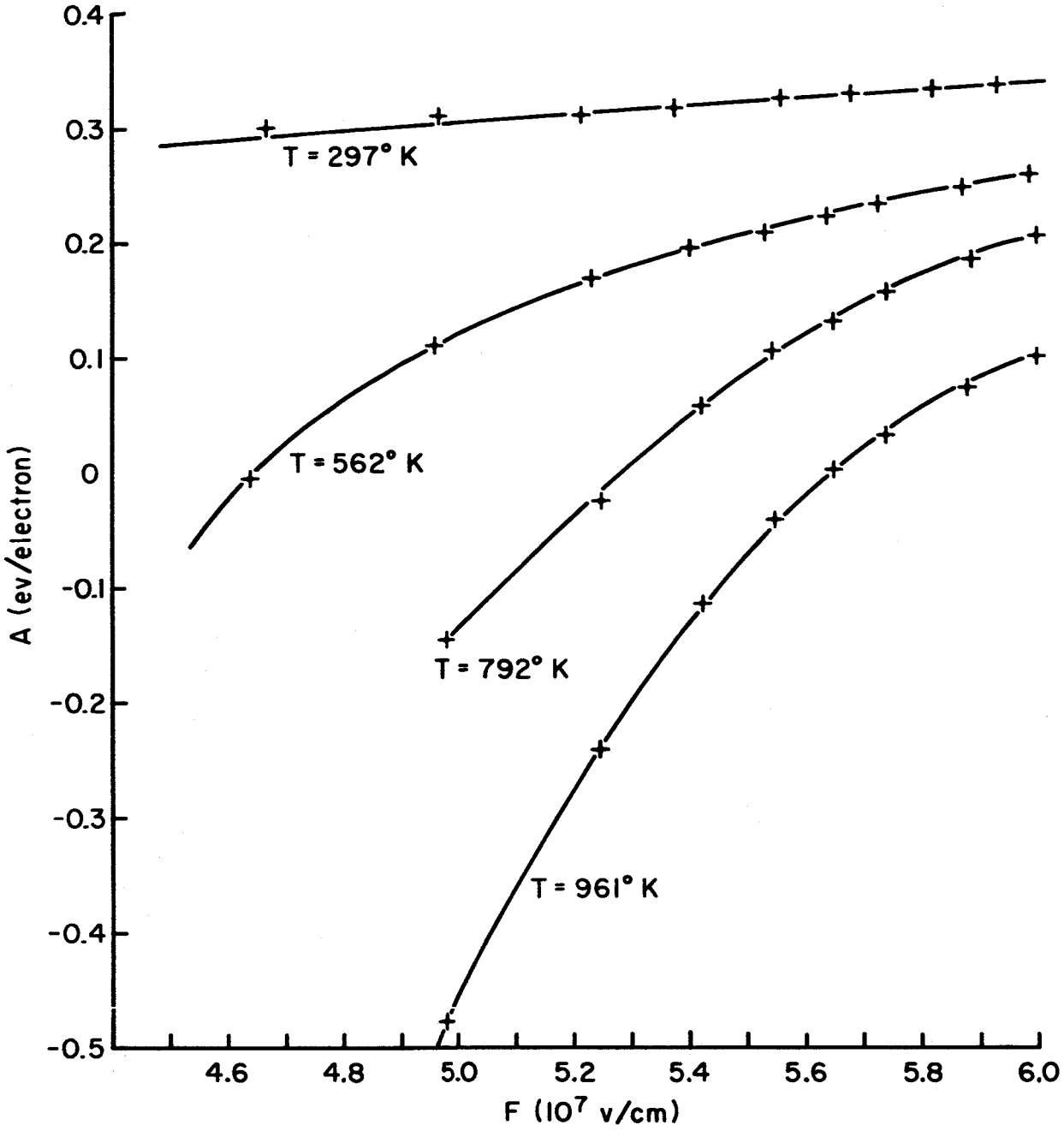

Figure 7. Experimentally determined energy exchange per electron A with the tungsten lattice as a function of applied electric field F at the indicated temperatures for clean tungsten. Negative values of A indicate emission cooling.

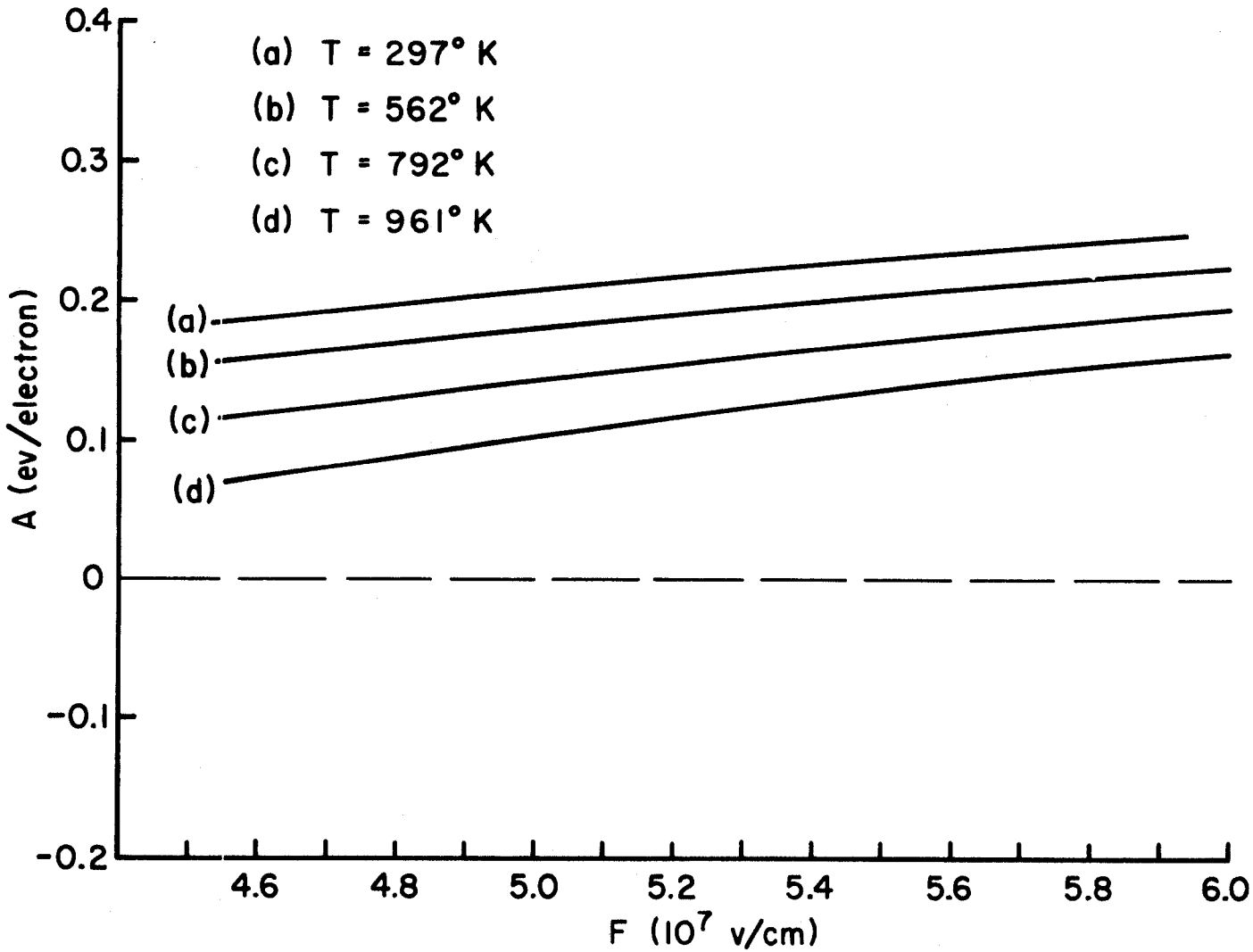

Figure 8. Calculated values of A for clean tungsten (ϕ = 4.52) according to equations (8) and (9) which correspond to the experimental results given in Figure 7.

that throughout the range of electric fields investigated the experimental inversion temperature is a factor of 1.5 to 2.0 below the theoretical values.

These latter results are somewhat different from those reported earlier[2] where the experimental results were generally higher than the calculated values throughout the temperature range and the occurrence of abnormally low inversion temperatures were not detected. It is believed that the reason for the higher values of A and T^* reported earlier stems from an increase in power input at the emitter structure by a back bombardment of ions formed at the collector plates by electron impact desorption. More rigorous outgassing of the collector plates employed in the obtaining of the present results should eliminate this problem.

We have been unable to account for the deviation from theory noted in the Nottingham effect results by possible artifacts of the method. For example, all the primary sources of experimental error mentioned earlier are in the direction which would increase, rather than decrease, the experimental values of A.

The emission heating results given earlier[2] for zirconium-coated tungsten also show reasonable agreement between the experimental and theoretical values of A for the 297°K results, although the results at higher temperatures show deviations from theory similar to those noted for the clean tungsten results.

Figure 6 gives the variation of T^* with F for zirconium on tungsten. As in the case of the clean tungsten, the inversion temperature varies linearly with field; however, the experimental values of T^* are similarly a

factor of 1.5 less than the calculated values. For example, at a field of 20 Mv/cm the experimental inversion temperature for a zirconium-coated tungsten emitter is approximately 410°K, whereas the corresponding value calculated by theory is 650°K.

In an attempt to explain the discrepancies between the experimental and predicted results of the Nottingham effect, one is led to examine the two basic premises of the theory. First; is the Sommerfeld-free electron model, upon which the total energy distribution theory is based, valid over the investigation field and temperature range? In view of the fair agreement between the energy distribution theory based on the free electron model and the results reported in Figures 3 and 4, and of the earlier investigations of Young and Müller[5] at low temperatures, one must conclude that discrepancies in the Nottingham effect cannot be attributed wholly to an inadequacy of the assumed free electron model. This conclusion is further supported by the near symmetrical energy distribution curve, for the 1059°K results of Figure 3 at F = 40.1 Mv/cm, which is in close agreement with theory. In contrast, the experimentally determined values of T^* for the clean tungsten results of Figure 7 is 320°K at F = 40.1 Mv/cm, which is a factor of 3.1 less than the predicted value of $T^* = 1040$°K.

The second and remaining basic premise of the Nottingham effect calculations which may be questioned is the assumption that the replacement electrons which fill the holes created by the emitted electrons originate at the Fermi level. In spite of the above evidence that the free electron model for tungsten is valid, as far as field emission theory is concerned, there is

also strong evidence from solid state measurements that the free electron model applies very poorly to tungsten. Measurements of the magneto-resistance[6] and high frequency surface conductance[7] of tungsten indicate that the Fermi surface areas are much less than for a free electron sphere containing 6 electrons per atom, and that an overlapping band model with equal numbers of electrons and holes more adequately describes the results. In addition, the positive Hall coefficient for tungsten is convincing evidence that electronic conduction occurs primarily by holes. Such deviation from the free electron model, which may not be easily detected by the observations of total energy distributions, could greatly alter the Nottingham effect by causing holes created by the emitted electrons to be filled by electrons considerably below the Fermi level. For example, if the average level of the conduction holes in tungsten are ϵ' below the Fermi level at a given temperature, then the inversion temperature would occur when the average energy (relative to the Fermi level) of the emitted electrons equals ϵ', rather than 0 as was assumed in the case of replacement electrons originating at the Fermi level. Additional measurements of the Nottingham effect in metals with negative Hall coefficients will be helpful in determining the importance of hole conduction in altering the results.

ANALYSIS OF "SINGLE PLANE" WORK FUNCTION VS. CESIUM COVERAGE DATA

The work function change (WFC) on the (100) and (110) planes of tungsten at various cesium coverages has been reported recently under other support[1]. In this section a review of the results and their interpretation will be given.

RESULTS ON (100) AND (110) TUNGSTEN

The probe tube utilized for the WFC analysis is shown in Figure 9 and consists of a tip assembly, cesium source and reservoir, anode electrode containing a small aperture, suppressor electrode and Faraday cage collector. An oxygen source has also been incorporated for future co-adsorption studies. Emitter tips were fabricated with (110) and (100)-oriented wire in order to eliminate large displacements of the tip assembly bellows to measure emission from these planes. Emission currents through the aperture as low as 10^{-14} amps could be measured using a Cary vibrating reed electrometer and careful shielding. During measurements of the I-V characteristics the emitter and suppressor voltage were held at -45 and -20 volts, respectively. The geometry of the tube was such that emission was accepted from a surface area roughly 100 A in diameter; thus emission is accepted from only well-defined local planes when well centered on the desired plane.

The experimental method of obtaining the average cesium surface concentration at each work function measurement has been described elsewhere[8]. The value of the work function ϕ for the (100) and (110) planes showed a dependency on the annealing temperature. That is, after flashing at high temperatures, work functions as low as 4.57 and 5.70 ev were obtained for the (100) and (110) planes respectively, whereas prolonged annealing at approximately 1050°K for several minutes led to work function measurements as high as 4.75 and 6.30 ev for the respective planes. This type of behavior has been reported earlier[9] and has been attributed to

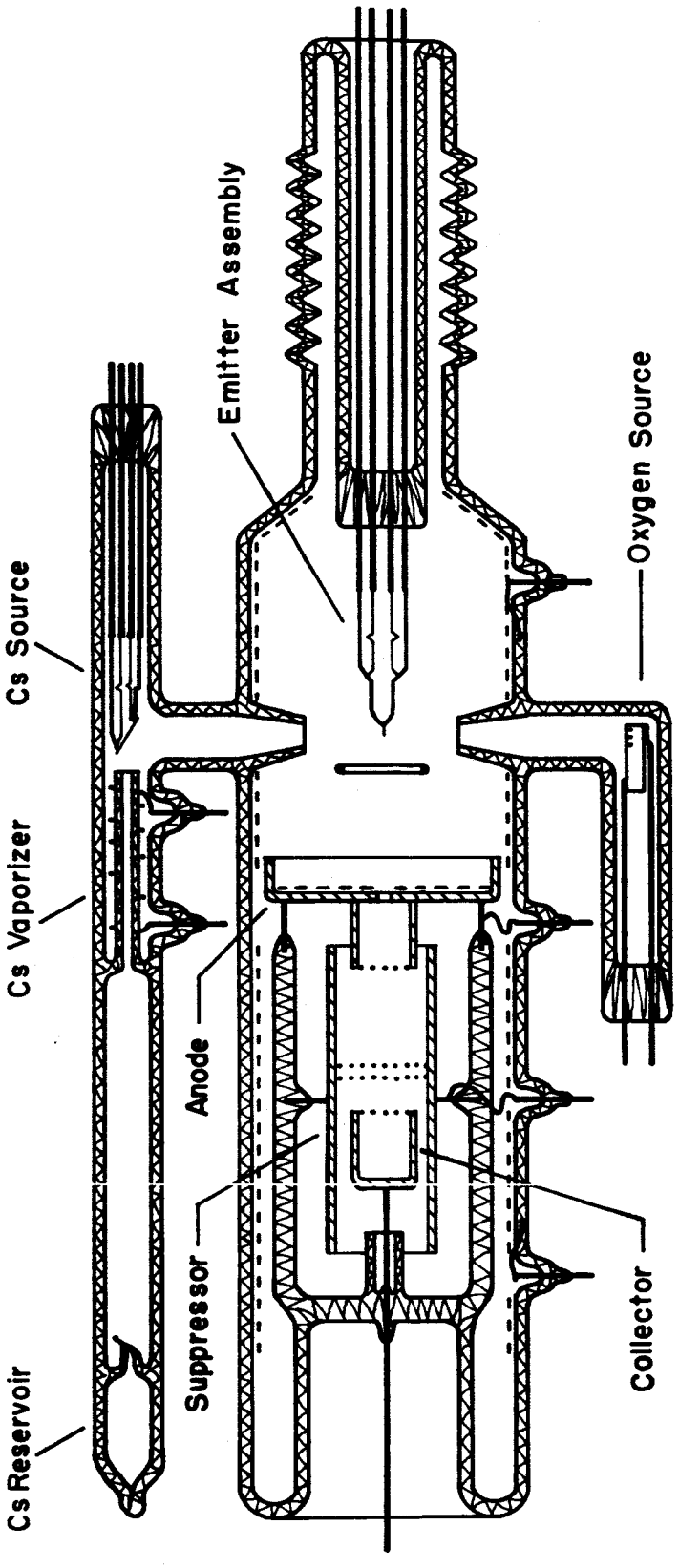

Figure 9. Probe tube for measuring field emission and work function of single crystallographic planes for various coverages of cesium and/or oxygen.

"frozen" thermal disorder of surface atoms which can be reduced by prolonged annealing at lower temperatures. In other words, the more atomically rough surface obtained after a high temperature flash exhibits a lower work function than does the same plane after prolonged annealing which leads to a more atomically smooth surface.

The results of the work function change $\Delta\phi$ on the (100) and (110) planes of tungsten as a function of average coverage are given in Figure 10 along with the average work function variation. It should be emphasized that the measurement of the atom density σ is based on an assumption of uniform coverage over the hemispherical emitter, so that any deviations from average σ on a given crystal plane will show up as some sort of a discontinuity in the $\Delta\phi$ vs. σ curve. Such discontinuities can be observed at low cesium coverages on both the (100) and (110) planes and are attributed to anisotropies in the coverage distribution for these two planes. It cannot be determined from this data whether the distribution of cesium becomes uniform at higher coverages, if it occurs at all.

In view of the uncertainty in the absolute cesium coverage on the various crystallographic planes, there is still some difficulty incurred in fitting these curves to various theories of WFC. We have suggested earlier[8,10] that several factors seem to indicate the occurrence of the monolayer condition at the knee of the $\Delta\phi$ vs. σ curves where ϕ no longer varies appreciably with coverage. This would be approximately 2.8 and 2.7×10^{14} atoms/cm^2 for the (100) and (110) planes, respectively. On the basis of geometric considerations only, the cesium monolayer coverage on the (100)

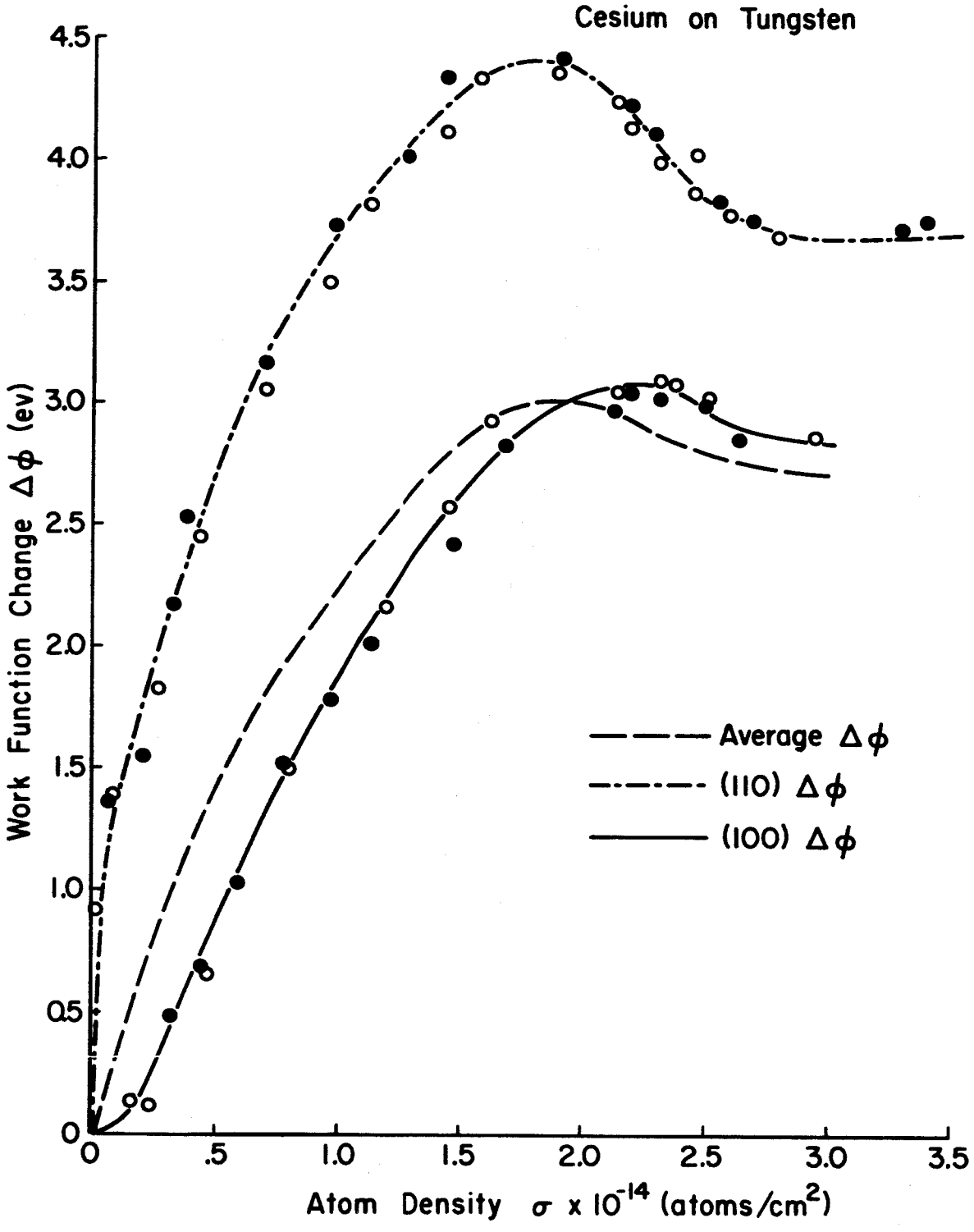

Figure 10. Work function change vs. average cesium atom density for the (110) and (100) planes of tungsten.

plane should be 2.5×10^{14}, whereas the monolayer coverage on the (110) plane should be 3.56×10^{14} atoms/cm^2. At this juncture there are two points of view which can be taken regarding the work function change with cesium coverage on the two planes: (1) the obvious shifting necessary on the two curves to cause linear extrapolation to zero coverage (which, according to Figure 10, is roughly 0.2×10^{14} atoms/cm^2 for the (110) plane and minus the same increment for the (100) plane in the low coverage range) must be such at high coverage to cause a monolayer coverage of 3.6 and 2.5×10^{14} atoms/cm^2 for the (110) and (100) planes, respectively; the other view is to assume that the monolayer condition is in fact nearly identical on both planes, namely $\sigma_o = 2.7 \times 10^{14}$ atoms/cm^2 and the anisotropy in the coverage distribution apparent at low σ disappears as σ approaches zero. There is no doubt that the discontinuity apparent in the low coverage region in the two curves of Figure 10 is due to anisotropies in the coverage distributions, since dipole moments calculated from the slopes of the curves at near-zero coverage would be inexplicably high for the (110) and low for the (100) plane.

The likely explanation for the anisotropy in the coverage distribution is the greater site density and binding energy for cesium on the (110) plane. At high coverages the binding energy should become more uniform over the different crystallographic planes so that the coverage distribution should be largely determined by the local site density and lateral interactions. As will be shown below, there is some evidence to believe that the atom density at the minimum work function is identical on the two planes; to accomplish

the latter a uniform shift of 0.2×10^{14} atoms/cm^2 in the proper direction throughout the coverage range for the curves both aligns the minimum work functions of the two curves and causes linear extrapolation to $\Delta\phi = 0$ as σ approaches zero, as mentioned above. This shift also leads to the occurrence of the work function minimum at $\sigma_m = 2.03 \times 10^{14}$ atoms/cm^2 for each curve. In addition, the monolayer coverage for the (110) and (100) planes occurs at 3.00 and 2.53×10^{14} atoms/cm^2 respectively. It is interesting to note that this amount of shifting yields a monolayer coverage on the (100) plane which is in agreement with a hard sphere geometric arrangement, whereas the monolayer coverage on a (110) plane is approximately 16% less than the geometric monolayer.

COMPARISON WITH THEORY

On the basis of the WFC data for the two planes with the above-mentioned corrections to the two curves an attempt will be made to fit the data to existing theories of WFC on adsorption. The basic Helmholtz equation relating $\Delta\phi$ and fractional monolayer coverage θ for a layer of adsorbate atoms with charge ze concentrated at a point d_o from the plane of electric neutrality is as follows:

$$\Delta\phi = 4\pi z e d_o \sigma_o \theta \qquad (10)$$

In the above formulation the dipole moment μ is given by $2 z e d_o$. The modification of equation (10) most frequently utilized to analyze $\Delta\phi$ vs. σ data allows for the de-polarization of the dipole moments by the dipole field of

neighboring adsorbate atoms. For a square array of adsorbate atoms of polarizability a which expands uniformly as the coverage decreases, the modification of equation (10) to include de-polarization effects is as follows:

$$\Delta\phi = \frac{2\pi\mu\sigma_o\theta}{\epsilon} \tag{11}$$

where:

$$\epsilon = 1 + 9a(\sigma_o\theta)^{3/2} \tag{12}$$

Equation (11) can be derived from application of Gauss' law to a Helmholtz dipole layer with a σ dependent dielectric constant ϵ. In the case of image dipoles $\Delta\phi$ is half the potential difference between the surface and free space at large distances from the surface. It can readily be shown that values of $\Delta\phi_m$ and θ_m at the maximum in the curve of $\Delta\phi$ vs. σ as given by equation (11) are as follows:

$$\theta_m = \left(\frac{2}{9a}\right)^{2/3} \frac{1}{\sigma_o} \tag{13}$$

$$\Delta\phi_m = 0.489\pi\mu a^{-2/3} \tag{14}$$

Thus, equations (13) and (14) permit calculations of a and μ for each plane from knowledge of the corresponding σ_m and $\Delta\phi_m$. Using the corrected curves of Figure 10 (i.e., $\sigma_m(100) = \sigma_m(110)$) the following values of a and μ are obtained:

$$a(110) = a(100) = 79\ A^3$$
$$\mu(110) = 15.8 \times 10^{-18}\ esu$$
$$\mu(100) = 11.1 \times 10^{-18}\ esu$$

Inserting the above values for α and μ into equation (11), the data of Figure 10 can be tested throughout the coverage range according to the depolarization theory. Regardless of whether the corrected or uncorrected data of Figure 10 is utilized, the simple depolarization theory as outlined above fails to fit the experimental data throughout an appreciable part of the coverage range.

Although various modifications of equation (10) to include depolarization effects have been given[11], a recent self-consistent treatment by MacDonald and Barlow[12] appears to be most rigorous. They consider the depolarizing field at a given adsorbed element arising from the total polarization of all surrounding elements including the presence of average charge on the adsorbing surface. A distinction is made in their treatment between "natural" fields E_{nl} polarizing a single adsorbed element in the absence of neighboring elements, and of the self-consistent effective field leading to induced polarization perpendicular to the adsorbent surface. For image dipoles they obtained the following expression:

$$\Delta\phi = 4\pi \sigma_o \theta \left[\frac{2 z e d_o}{\epsilon} - \frac{4\pi \theta \sigma_o z e \alpha}{\epsilon} + \frac{\alpha \bar{E}_{nl}}{\epsilon} - z e d_o \right] \quad (15)$$

In the case of polarized atomic adsorption z = 0 and equation (15) is identical to equation (11) where $\mu = 2\alpha E_{nl}$ (the factor 2 arises from the fact that μ is totally contained in the ad-atom). In the case of image dipoles with small α, $\epsilon \cong 1$ and αE_{nl} is small compared to the other terms throughout the range of θ and equation (15) becomes:

$$\Delta\phi = 4\pi\theta\sigma_o ze\, d_o - (4\pi\theta\sigma_o)^2 ze\, a \qquad (16)$$

It can readily be shown that $\Delta\phi_m$ occurs at:

$$\theta_m = \frac{d_o}{8\pi\sigma_o a} \qquad (17)$$

The corrected data of Figure 10 has been plotted in Figure 11 according to equation (16) written in the form:

$$\frac{\Delta\phi}{\theta} = B - C\theta \qquad (18)$$

where

$$\frac{C}{B} = \frac{1}{2\theta_m} = \frac{4\pi\sigma_o a}{d_o} \qquad (19)$$

The agreement of the experimental data with equation (18), as shown in Figure 11 for the (110) and (100) results, lends support to MacDonald's theory of WFC. Using the data of Figure 10 and equation (18) without any corrections to σ causes the low θ points to deviate upwards; however, the slope and intercept of the line drawn through the higher coverage points are nearly unchanged from the corrected data used in Figure 11. Good agreement near $\theta = 1$ is somewhat fortuitous since the approximation that $\epsilon \cong 1$ becomes less valid. The various constants of equation (16) obtained from the slopes and intercepts of curve I and II of Figure 11 are given in Table I. The ratio $zd_o(110) / zd_o(100) = 1.48$ is interestingly close to the ratio of the respective substrate work functions, namely $\phi_{110}/\phi_{100} = 1.29$.

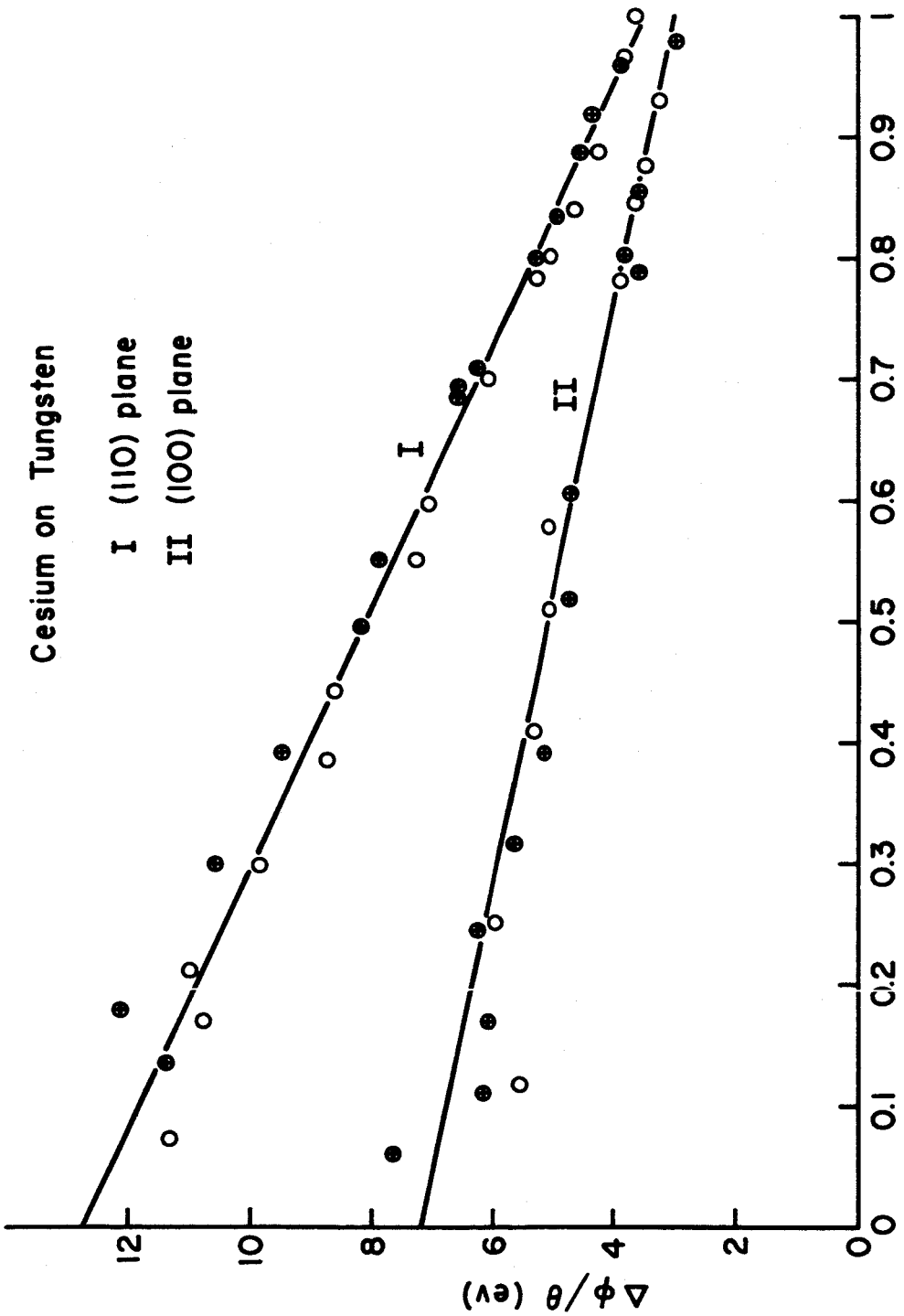

Figure 11. Analysis of the data of Figure 10 according to equation (18).

TABLE I

Constants of equation (16) obtained from best fit to data of Figure 10

Plane	$ze\,d_o$ (esu)	$z\,d_o$ (A)	a/d_o (A^2)	$a\,z$ (A^3)
(110)	11.2×10^{-18}	2.34	1.95	4.56
(100)	7.6×10^{-18}	1.58	1.84	2.90

From equations (16) and (17) one finds that $\Delta\phi_m$ is given as follows:

$$\Delta\phi_m = \frac{ze\,d_o^2}{4a} = \frac{\mu\,d_o}{8a} \tag{20}$$

In view of the following relation obtained from Table I,

$$\frac{a/d_o\,(110)}{a/d_o\,(100)} = 1.06 \tag{21}$$

it appears that $\Delta\phi_m$ given by equation (20) is proportional to μ. Although it is not totally justified with the limited probe data, let us assume the existence of a linear relationship between μ and ϕ_s of the form:

$$\mu = k(\phi_s - \phi_a) \tag{22}$$

where ϕ_a is the work function of the adsorbate; one might then expect to observe the following relationship:

$$\Delta\phi_m = k'(\phi_s - \phi_a) \tag{23}$$

If the proportionality of constant k' is near unity, then one obtains the prediction that ϕ_m depends only on the adsorbate properties, namely ϕ_a, and is independent of the substrate electrical and geometric properties. The

latter is indeed observed experimentally for cesium on a variety of substrates and different crystallographic planes of a given substrate in which ϕ_s varies from 4.65 to 6.00 ev. It was also pointed out in an early report[1] that equation (23) seems to be approximately valid for a variety of substrate-adsorbate combinations.

In essence, the preceding discussions point out the likelihood of a linear relation between μ and ϕ_s for a given adsorbate which, when combined with the predictions of MacDonald's WFC theory (equation 20), yields an expression (equation 23) that is experimentally confirmed.

It is also interesting to compare the values of z and α on the (100) and (110) planes since their value gives insight as to the electronic structure of the ad-atom. From Table I it can be deduced that:

$$\frac{\alpha\, z\ (110)}{\alpha\, z\ (100)} = 1.57 \qquad (24)$$

In view of the large value of ϕ_{110} it is likely that $z \tilde{=} 1$, thereby according to Table I, yielding a value of $\alpha_{110} = 4.56\ A^3$ and $d_{110} = 2.34$ A. It also follows that $z_{100} = 0.634$ and $d_{100} = 2.48$ A if $\alpha_{110} = \alpha_{100}$. The nearly identical values of d_{100} and d_{110} may mean the image plane is further from the geometrical surface on the (100), but is compensated by the fact that cesium can "bury" itself further into a (100) than a (110) surface; thus, the larger value of μ on the (110) is primarily due to a larger z.

Table II compares the values of α, z, and d_o as obtained above on the (100) and (110) planes with atomic and ionic parameters of cesium. It seems somewhat paradoxial that α of the ad-atom is close to α of cs^+ whereas

d_o of the ad-atom is close to the metallic radius; furthermore, the results of Table II suggest a large variation in z of the ad-atom with crystal plane without concomitant variations in α or d_o. Although values of α, d_o and z given in Table II are based on equivocal assumptions, they do reflect the current ideas of metallic adsorption. For example, the strong overlap of the atomic orbital of cesium with metallic wave functions leads to a broadening of the valence level A in the adsorbed state. On the (110) plane the large value of $I-\phi$, where I is the ionization potential of the adsorbate, may cause the broadened valence level to lie wholly above the Fermi level of the substrate, so that a negligible part of the A band is filled, i.e., $z \cong 1$. For all other planes which possess relatively small $I-\phi$ the value of z is appreciably less in unity.

TABLE II

Various constants obtained from Table I results assuming $z_{110} = 1$ and $\alpha_{110} = \alpha_{100}$

	α (A^3)	d_o (A)	z
Cs	48[a]	2.62	0
Cs-W (100)	4.56	2.48	0.63
Cs^+	2.80[b]	1.69	1
Cs-W (110)	4.56	2.34	1

a - Ref. 13; b - Ref. 14

ADSORBATE POLARIZABILITY

An independent method of estimating the value of α in the adsorbed state as a function of θ is possible by analysis of the variation of the pre-exponential factor of the Fowler-Nordheim equation. This stems from a field-induced WFC, which according to equation (15) would involve an additional term:

$$\Delta\phi_F = \frac{4\pi\theta\sigma_o F}{\epsilon} \tag{24}$$

where the ratio of the effective field F_0 to the external field F is $F/F_0 = \epsilon$. Incorporating this effect into the Fowler-Nordheim equation (4) yields:

$$\ln\frac{I}{V^2} = \ln\frac{B}{\phi_F t^2(y)} - \frac{b\,\phi_F^{3/2}\,v(y)}{\beta V} \tag{25}$$

where $b = 6.8 \times 10^7$ when I is in amperes, F in volts/cm, and ϕ in ev. B is a function of the geometric factor β where $F = \beta V$. Noting that $\phi_F^{3/2} = (\phi_o + \Delta\phi_F)^{3/2}$ can be expanded, since $\Delta\phi$ is normally small compared to ϕ_o, and using the empirical relation $v(y) = 0.943 - 0.146 \times 10^{-6} F/\phi^2$, we can rewrite equation (25) as follows:

$$\ln\frac{I}{V^2} = \ln\frac{B}{\phi_F t^2(y)} + \frac{9.94}{\phi_F^{1/2}} - 5.66\, b\pi\sigma_o\theta\phi_o^{1/2}\alpha - 0.943\,\frac{b\phi_o^{3/2}}{\beta V} \tag{26}$$

Within limits of the above approximation the experimental intercept ln A of the Fowler-Nordheim plot ($\ln I/V^2$ vs. $1/V$) is given by:

$$\ln A = \ln \frac{B}{\phi_F t^2(y)} + \frac{9.94}{\phi_F^{1/2}} - 5.66 b\pi \sigma_o \phi_o^{1/2} \frac{a}{\epsilon} \qquad (27)$$

It is now possible to obtain the following expression for a/ϵ:

$$\frac{a}{\epsilon} = \frac{\log \frac{\phi_s t_s^2(y)}{\phi_F t^2(y)} - \log \frac{A}{A_s} + 4.32\left(\frac{1}{\phi_F^{1/2}} - \frac{1}{\phi_s^{1/2}}\right)}{1.67 \times 10^8 \pi \sigma_o \theta \phi_o^{1/2}} \qquad (28)$$

where ϕ_s and A_s refer to the corresponding clean values. Values of a/ϵ and a are given in Table III for the (110) and (100) as a function of σ. Since relatively large experimental errors are associated with the log A/A_s term in the numerator of equation (28) along with uncertainties in $\sigma_o \theta$, one must consider the values of a as a rough approximation. The two conclusions to be drawn from the results are: (1) the values of a appear relatively constant over the range of σ; and (2) the values of a are roughly similar for the two planes and in approximate agreement with the value 4.5 A^3 obtained in the preceding section by assuming $z_{110} = 1$.

TABLE III

Polarizabilities of the adsorbed cesium atoms on two crystallographic planes of tungsten calculated according to equation (28)

(100)					(110)				
$\sigma^*(\times 10^{14})$	ϕ(ev)	$a/\epsilon(A^3)$	$a(A^3)$	$\ln A/A_o$	$\sigma^*(\times 10^{14})$	ϕ(ev)	$a/\epsilon(A^3)$	$a(A^3)$	$\ln A/A_o$
2.35	1.65	6.0	7.4	0.65	3.00	2.19	6.0	8.4	-0.09
2.16	1.63	4.3	4.9	1.07	2.90	2.13	4.6	5.8	0.42
2.03	1.61	5.9	6.9	0.89	2.66	2.03	4.2	5.0	0.73
1.97	1.67	5.7	6.7	0.83	2.52	1.91	5.5	6.8	0.63
1.53	1.84	4.9	5.3	0.94	2.40	1.76	6.3	8.0	0.72
1.31	2.22	3.2	3.3	0.81	2.35	1.65	5.6	6.9	1.03
0.97	2.61	5.9	6.2	0.36	2.10	1.54	5.5	6.5	1.34
0.80	2.87	5.0	5.1	0.34	1.79	1.57	6.1	7.0	1.34
0.62	3.13	3.8	3.9	0.34	1.65	1.79	6.9	8.0	0.97
0.28	3.93	4.5	4.5	0.08	1.34	2.09	5.2	5.6	1.01
0.16	4.17	29.0	29.0	-0.41	1.16	2.42	8.1	8.9	0.46
					0.90	2.85	8.5	9.1	0.28
					0.64	3.46	5.6	5.8	0.35
					0.29	4.51	1.0	1.0	0.31

*corrected values of σ used

SUMMARY

An analysis of the WFC data for cesium on the (110) and (100) planes of tungsten by simple depolarization theory appears inadequate and leads to values of $a = 79\ A^3$. The same data, analyzed according to MacDonald's theory for image dipoles, lead to much closer agreement with theory and yields the values of a in close agreement with those obtained by analysis of the pre-exponential of the Fowler-Nordheim equation, namely 5 to 7 A^3. The fact that ϕ_m is independent of substrate work function and geometry and only a function of adsorbate electrical properties occurs because of a compensating increase in the dipole moment μ as the work function of the substrate is increased.

FUTURE WORK

Further investigations of the Nottingham effect are being carried out with a thoriated tungsten emitter in order to vary work function continuously from 4.52 to 3.10 ev. An attempt to perform such a study with barium as the adsorbate met with failure because of the excessive mobility of barium at temperatures slightly above 300°K. It is expected that thorium will be somewhat more stable in this regard than barium.

Investigation of the total energy distribution of field emitted electrons from all the major planes of tungsten and as a function of field and temperature will be performed in order to ascertain possible clues as to the breakdown of the free electron model for tungsten.

It is also expected that investigations of the co-adsorption of cesium and oxygen by probe tube methods will be initiated in the near future.

FUTURE WORK

Further investigations of the Nottingham effect are being carried out with a thoriated tungsten emitter in order to vary work function continuously from 4.52 to 3.10 ev. An attempt to perform such a study with barium as the adsorbate met with failure because of the excessive mobility of barium at temperatures slightly above 300°K. It is expected that thorium will be somewhat more stable in this regard than barium.

Investigation of the total energy distribution of field emitted electrons from all the major planes of tungsten and as a function of field and temperature will be performed in order to ascertain possible clues as to the breakdown of the free electron model for tungsten.

It is also expected that investigations of the co-adsorption of cesium and oxygen by probe tube methods will be initiated in the near future.

REFERENCES

1. L. W. Swanson, et al., Quarterly Report No. 2 for NASA Contract NAS3-5902 (Field Emission Corporation, 1964).

2. L. W. Swanson and L. C. Crouser, Quarterly Report No. 1 for NASA Contract NASw-1082 (Field Emission Corporation, 1965).

3. R. Good and E. Müller, Handbuch der Physik 21, 176 (1956).

4. P. Levine, J. Appl. Phys. 33, 582 (1962).

5. R. Young and E. Müller, Phys. Rev. 113, 115 (1959).

6. E. Fawcett, Phys. Rev. 128, 1 (1962).

7. E. Fawcett and D. Griffiths, J. Phys. Chem. Solids 23, 1631 (1962).

8. L. W. Swanson et al., Final Report for NASA Contract NASw-458 (Field Emission Corporation, 1963).

9. E. Müller, J. Appl. Phys. 26, 732 (1955).

10. L. W. Swanson, et al., Final Report for NASA Contract NASr-19 (Field Emission Corporation, 1962).

11. E. Gyftopoulos and J. Levine, J. Appl. Phys. 33, 67 (1962).

12. J. MacDonald and C. Barlow, J. Chem. Phys. 39, 412 (1965).

13. G. Chamberlain and J. Zorn, Phys. Rev. 129, 677 (1963).

14. R. Sternheimer, Phys. Rev. 115, 1198 (1959).